Acta Materialia 242 (2023) 118427

Contents lists available at ScienceDirect

Acta Materialia

journal homepage: www.elsevier.com/locate/actamat

Unexpected dynamic transformation from α phase to β phase in zirconium alloy revealed by in-situ neutron diffraction during high temperature deformation

Baoqi Guo[a,*], Wenqi Mao[b], Yan Chong[a,*], Akinobu Shibata[c], Stefanus Harjo[b], Wu Gong[b], Huicong Chen[d,*], John J. Jonas[d], Nobuhiro Tsuji[a,e,*]

[a] Department of Materials Science and Engineering, Kyoto University, Yoshida-honmachi, Sakyo-ku, Kyoto 606-8501, Japan
[b] J-PARC Center, Japan Atomic Energy Agency, 2-4, Shirane Shirakata, Tokai, Ibaraki 319-1195, Japan
[c] Research Center for Structural Materials, National Institute for Materials Science (NIMS), 1-2-1, Sengen, Tsukuba 305-0047, Japan
[d] Department of Materials Engineering, McGill University, 3610 University St., Montreal H3A 0C5, Canada
[e] Elements Strategy Initiative for Structural Materials (ESISM), Kyoto University, Yoshida-honmachi, Sakyo-ku, Kyoto 606-8501, Japan

ARTICLE INFO

Article history:
Received 13 April 2022
Revised 23 August 2022
Accepted 11 October 2022
Available online 14 October 2022

Keywords:
Dynamic transformation
Hot deformation
Zirconium alloy
In-situ neutron diffraction

ABSTRACT

Dynamic transformation from alpha (HCP) to beta (BCC) phase in a zirconium alloy was revealed by the use of in-situ neutron diffraction during hot compression. The dynamic transformation was unexpectedly detected during isothermal compression at temperatures of 900°C and 950°C (alpha + beta two-phase region) and strain rates of 0.01 s^{-1} and 0.001 s^{-1}, even though equilibrium two-phase states were achieved prior to the hot compression. Dynamic transformation was accompanied by diffusion of Sn from beta to alpha phase, which resulted in changes of lattice parameters and a characteristic microstructure of alpha grains. The lattice constant of alpha phase measured by the in-situ neutron diffraction increased during the hot compression, while the lattice constant of beta phase exhibited an initial increase and subsequent decrease during the hot compression. As a result, the magnitude of lattice (elastic) strain as well as stress (elastic stress, or phase stress) in alpha phase was found to become much greater than those in beta phase. According to an atomistic simulation, the Gibbs free energy of alpha phase increased with hydrostatic compressive pressure more evidently than that of beta phase. It could be concluded from such results that the occurrence of the dynamic transformation from alpha to beta is attributed to an increase in the Gibbs free energy of alpha phase relative to beta phase owing to the difference in the phase stress; i.e., the larger lattice distortion made alpha phase thermodynamically more unstable than beta phase. The present result suggests that deformation of two-phase materials can dynamically make Gibbs free energy of plastically harder phase higher than that of the softer phase through increasing elastic energy in the harder phase, which might lead to dynamic transformation from harder phase to softer phase.

1. Introduction

Dynamic transformation is the phase transformation happening during deformation [1,2]. Dynamic transformation of austenite phase with face centered cubic (FCC) crystal structure to ferrite phase with body centered cubic (BCC) structure in steels was first reported by Yada et al. [3] using in-situ X-ray diffraction testing during deformation at high temperatures. The dynamic transformation can enhance toughness and strength of steels by producing ultrafine grains [4–7]. It has been argued that the nucleation of product phase in dynamic transformation is activated displacively and nuclei grow diffusionally [1,8]. In case of titanium alloys, dynamic transformation from alpha phase having hexagonal close packed (HCP) crystal structure to beta phase (BCC) may lead to excellent superplasticity and improve tensile elongation. The dynamic transformation often contributes to stress accommodation and accounts for a large proportion of flow softening [9,10]. Hence, it is important to reveal the mechanism of dynamic transformation as well as its influence on hot deformation behaviors of metallic materials.

* Corresponding authors.
E-mail addresses: guo.baoqi.7z@kyoto-u.ac.jp (B. Guo), chong.yan.6w@kyoto-u.ac.jp (Y. Chong), huicong.chen@mail.mcgill.ca (H. Chen), nobuhiro.tsuji@me.com (N. Tsuji).

https://doi.org/10.1016/j.actamat.2022.118427

In titanium alloys, dynamic transformation during hot deformation was first predicted by Gegel and Nadiv [11] in a Ti-6Al-2Sn-4Zr-2Mo alloy. Later it was observed in near alpha and two-phase titanium alloys by the use of ex-situ technique in which phase fractions were measured at ambient temperature after hot deformation and rapid cooling. For example, Prada et al. [12] showed that the beta phase fraction in a Ni modified Ti-6Al-4V alloy increased gradually during straining from strain of 0 to 1.65 at 815°C that corresponded to alpha + beta two-phase region. Later Koike et al. [13] reported an evident increase in beta phase fraction during tensile testing of a Ti-5.5Al-1Fe alloy at temperatures ranging from 777°C to 927°C (alpha + beta two-phase region). Specifically, the beta phase percentage increased from 15% prior to deformation to 41% after deformation to a strain of 1.6 at a strain rate of 10^{-3} s^{-1} at 827°C. Recently, dynamic transformation was observed during hot compression of a near alpha titanium alloy (IMI 834). The beta phase percentage increased by 20% during deformation to a strain of 1.0 at a strain rate of 0.01 s^{-1} and 1000°C (two-phase region). It was concluded that the flow softening observed was attributed to the dynamic transformation observed, because newly formed beta phase was softer than alpha at deformation temperature [14]. However, as the ex-situ observations were used in the aforementioned works, the observed microstructures might include static phase transformation (e.g., beta to alpha) during unloading and quenching even though rapid cooling was taken. The ex-situ observations make it difficult to accurately characterize the phase components during hot deformation. In addition, martensitic phase transformation of beta during quenching makes it impossible to study the phase status and microstructures at elevated temperatures. As a result, the mechanism of dynamic transformation has not been fully clarified yet.

Previous works regarding dynamic transformation have focused mainly on steels and titanium alloys. Recently, It has been predicted [2,14] that dynamic transformation is likely to take place in zirconium alloys having similar phase diagrams and crystal structure phases to titanium alloys. The present work aimed to clarify dynamic transformation behavior of a zirconium alloy for the first time, using in-situ neutron diffraction during hot deformation. It is expected that the present investigations can throw light on the real-time transformation characteristics at high temperatures. The driving force of dynamic transformation has been revealed for the first time, on the basis of neutron diffraction results in the current study.

2. Experimental

The material used in the present study is a Zircaloy-4 alloy with a composition of 1.5 Sn, 0.21 Fe, 0.1 Cr, 0.12 O (in weight percent), and balanced Zr. The initial material at room temperature was characterized to have full alpha phase with an equiaxed grain structure. Transus temperatures between alpha single-phase region and alpha + beta two-phase region, and alpha + beta two-phase region and beta single-phase region of the alloy were 810°C and 980°C, respectively. A physical simulator for thermo-mechanical processing was equipped in the beam line (BL) 19 "TAKUMI" of the Materials and Life Science Experimental Facility (MLF) at Japan Proton Accelerator Research Complex (J-PARC). The schematic diagram of the facility for the in-situ neutron diffraction during hot compression is shown in Fig. 1(a) [7]. A white pulsed neutron beam was irradiated to the cylindrical compression specimen and diffraction information was collected by two neutron detectors set at opposite positions perpendicular to the direction of incident neutron beam. The height and width of the incident beam were 5 mm and 5 mm. The dotted area in Fig. 1(a) denoted the thermo-mechanical processing simulator, in which a compression deformation system with two anvils as well as induction heating system were installed. A thermocouple was welded on the side surface of the specimen to track the temperature of the specimen during processing. In Fig. 1(b), the lattice planes parallel to the compression axis which produce diffraction are illustrated. The neutron diffraction was collected from the starting time of initial heating to the end of the hot deformation. In order to obtain peak positions and integrated intensities, diffraction peaks were fitted using Voigt function. The volume fraction of BCC beta phase was measured according to the equation given by:

$$V_{BCC} = \frac{\frac{1}{n}\sum_{j=1}^{n}\frac{I_{BCC}^{j}}{R_{BCC}^{j}}}{\frac{1}{n}\sum_{j=1}^{n}\frac{I_{BCC}^{j}}{R_{BCC}^{j}} + \frac{1}{n}\sum_{j=1}^{n}\frac{I_{HCP}^{j}}{R_{HCP}^{j}}} \quad (1)$$

Here I_{BCC}^{j} and I_{HCP}^{j} denote the integrated intensity of any diffraction peak of BCC (beta) and HCP (alpha) phases, respectively. R represents the material scattering factor, and n is the number of peaks used for the phase fraction calculation. Phase fractions were calculated through considering multiple peaks in each phase to minimize the effects of texture on peak intensity. Six peaks of HCP and five peaks of BCC were detected during holding at 900°C for 20 min prior to deformation as shown in the supplementary material (**Fig. S1**). Three peaks of alpha phase (i.e. (002), (101), (102)) and three peaks of beta phase (i.e. (110), (200), (211)) were used to calculate phase fractions according to Eq. (1). Evolution of the texture was analyzed by using the MAUD (material analysis using diffraction) program. The spherical harmonics model with assuming a fiber texture along the compressive direction was used, and the analysis was based on eighth-order harmonic function. It was demonstrated that texture of BCC was very weak with a slight increase in (101) direction after hot deformation (**Fig. S2**). Lattice elastic strain ε_{hkl} is expressed by:

$$\varepsilon_{hkl} = \frac{d_{hkl} - d_0}{d_0} \quad (2)$$

where d_0 is the reference lattice spacing measured under the free of stress condition, d_{hkl} is the lattice spacing of (hkl) plane during the deformation. Relations between lattice constants of alpha and beta phases and interplanar spacing d_{hkl} are given by: $1/d_{hkl}^2 = 4(h^2+hk+k^2)/3a^2 + l^2/c^2$ and $1/d_{hkl}^2 = (h^2+k^2+l^2)/a^2$, respectively.

The alloy was machined into cylindrical compression specimens with height of 11 mm and diameter of 6.6 mm. Mica sheets were applied to the top and bottom surfaces of the samples as a heat insulator. A nitrogen gas atmosphere was used to minimize oxidation during the hot compression in a chamber. The specimens were heated at 2°C s^{-1} to a compression temperature and then held for 20 minutes prior to deformation for homogenizing temperature of the specimen. The specimens were uniaxially compressed to a logarithmic compression strain of 0.7 at a strain rate of 0.01 s^{-1} or 0.001 s^{-1} at temperature of 900°C and 950°C. The specimens were water quenched immediately after the hot compression to preserve microstructures at elevated temperatures. Hot-compressed specimens were cut along the longitudinal direction and cut sections including the center position of the specimens were eletro-polished in a solution of 10 vol. % perchloric acid and 90 vol. % methanol at -40°C and 25 V for 90s. Microstructures of the specimens prior to and after the hot compression were characterized using a field-emission scanning electron microscope (FE-SEM) equipped with a back scattered electron (BSE) detector.

Dynamic transformation in pure zirconium was predicted by an atomistic simulation. Structural phase transformation is driven by the change in Gibbs free energy $G(p,T)$ that is determined as: G = H − TS. Here H, T and S denote the enthalpy, temperature and entropy of the system, respectively. Accordingly, the phase with the lowest Gibbs energy (or the lowest enthalpy at T=0 K) will be the

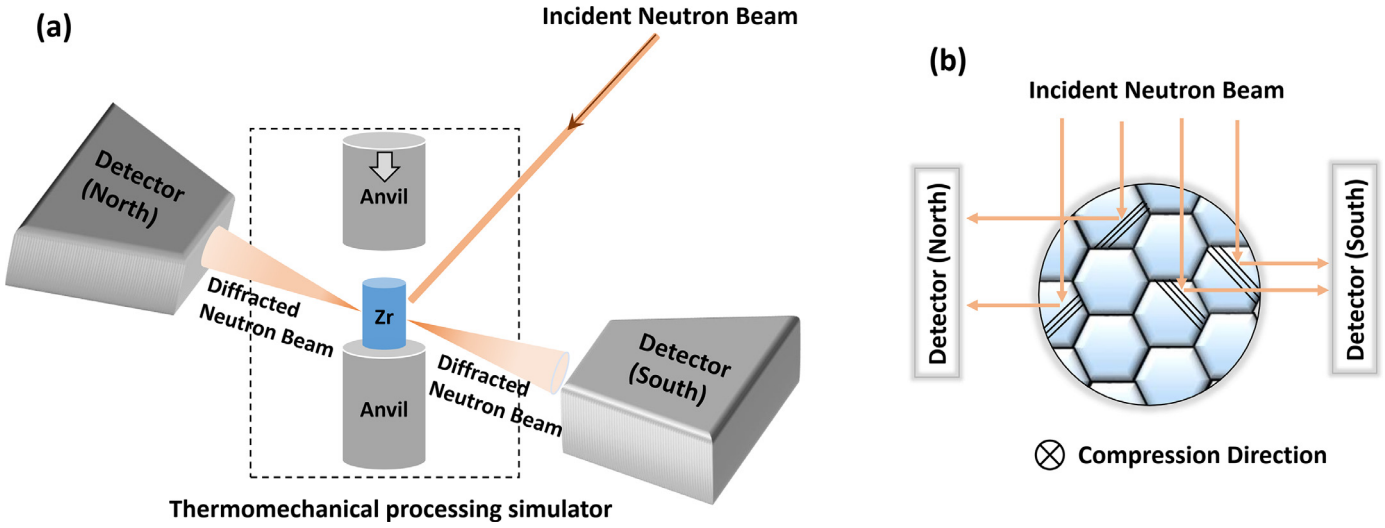

Fig. 1. (a) Schematic diagram of the facility of the in-situ neutron diffraction during hot compression settled at BL19 of J-PARC. (b) Geometric relationships between incident white neutron beam and lattice planes as well as the compression axis.

thermodynamically stable phase at a given condition (p, T). In order to calculate the Gibbs energy for dynamic transformation in zirconium, atomistic simulations were performed using the open-source parallel molecular dynamics code LAMMPS [15]. The interatomic interaction was calculated by an embedded atom method (EAM) potential [16]. A prefect hcp-Zr single crystal with cubic simulation shape (675,840 atoms) with the X, Y and Z axes parallel to [-2110], [01-10] and [0001] crystallographic directions, or a bcc-Zr single crystal (628,864 atoms) with the X, Y and Z axes parallel to [100], [010] and [001] crystallographic directions, respectively. Periodic boundary conditions were applied along three directions for simulating the effect of hydrostatic compressive pressure on the phase stability between alpha and beta phases in pure Zr, removing any influence of surface or edge effects. All samples were minimized initially using the conjugate gradient method [17]. Then, hydrostatic compression stress was applied by rescaling the atomic coordinates at T=0 K and the total energy E_{tot} was calculated in strained sample. Average energy for each atom was calculated as $H_{atom} = E_{tot}/N$, where N is the number of atoms in each sample. In current calculation, the system with lower H_{atom} (thus lower G at 0 K) at a given pressure will be more stable and dominant in dynamic transformation of zirconium.

3. Results and discussions

3.1. Change of phase fractions (Direct observation of dynamic transformation)

Figure 2(a) shows a two-dimensional description of neutron diffraction profile of the Zr alloy obtained during the hot compression at 900°C at a strain rate of 0.001 s^{-1}. The time of flight (TOF) corresponds to the diffraction peak positions of two phases [18]. During holding at 900°C, alpha phase partially transformed to beta phase. For example, (110) peak of beta phase slightly increased during holding while intensities of (101) and (002) peaks of alpha phase decreased. But the intensities became almost constant during holding, which indicated the phase fractions reached the equilibrium values at this temperature. The fractions of alpha phase and beta phase calculated by Eq. (1) at the end of the isothermal holding for 20 minutes were 12.8% and 87.2%, respectively, which was comparable to the volume fractions at 900°C estimated from the theoretical equilibrium phase diagram [19]. This conformed that the phase fractions reached equilibrium before the hot-compression.

During isothermal compression, an evident increase in the intensity of beta phase, such as (110) peak of beta, was observed. Such variations of peak intensity were compared in Fig. 2(b) furthermore. It could be clearly seen that the intensity of (110) peak of beta phase increased while the intensities of (101) and (002) peaks of alpha phase decreased during hot-deformation, which could be recognized by comparing the blue curve (just before deformation) with the red curve (deformation: at 120 s) and black curve (deformation: at 300 s) in Fig. 2(b). Figure 2(c) is a three-dimensional plot of another in-situ neutron diffraction result during hot-compression at 950°C at a strain rate of 0.01 s^{-1}. A drastic increase in the intensity of beta phase during hot compression could be observed again at this higher temperature. In Fig. 2(d), it is confirmed that the intensity of alpha (101) and (002) peaks decreased, while the intensity of beta (110) peak increased from the stage of just before deformation (red curve) to the stage of deformation (black curve).

The results shown in Fig. 2, i.e., the decrease of alpha peaks and the increase of beta peak suggest the occurrence of dynamic transformation from alpha phase to beta phase during hot deformation. However, the peak intensities can be affected by crystal rotation during deformation. All major diffraction peaks before and after the hot compression at 900°C at a strain rate of 10^{-3} s^{-1} are shown in **Fig. S1** in the supplementary materials. The intensities of all alpha peaks decreased, while the intensities of most beta phase decreased. Exceptionally, the intensity of (200) beta decreased by the hot deformation, which might be caused by the crystal rotation during hot-compression as BCC metals and alloys tend to form a fiber texture with <100> + <111> parallel to the compression direction in compression. However, the pole figures (**Fig. S2** in the supplementary materials), which was reconstructed by MAUD (material analysis using diffraction) program, did not show strong textures both in alpha and beta phases. Therefore, it is considered that the changes of peak intensities were not dominated by crystal rotation or texture formation during deformation.

In Fig. 3(a), changes of the diffraction peak intensity normalized by the intensity at the initial unloaded state are plotted as a function of the deformation time. The normalized intensities of (110) and (211) peaks of beta phase increased during hot-deformation. In contrast, the normalized intensity of (101) peak of alpha phase decreased during the deformation. The intensities of (002) peak of

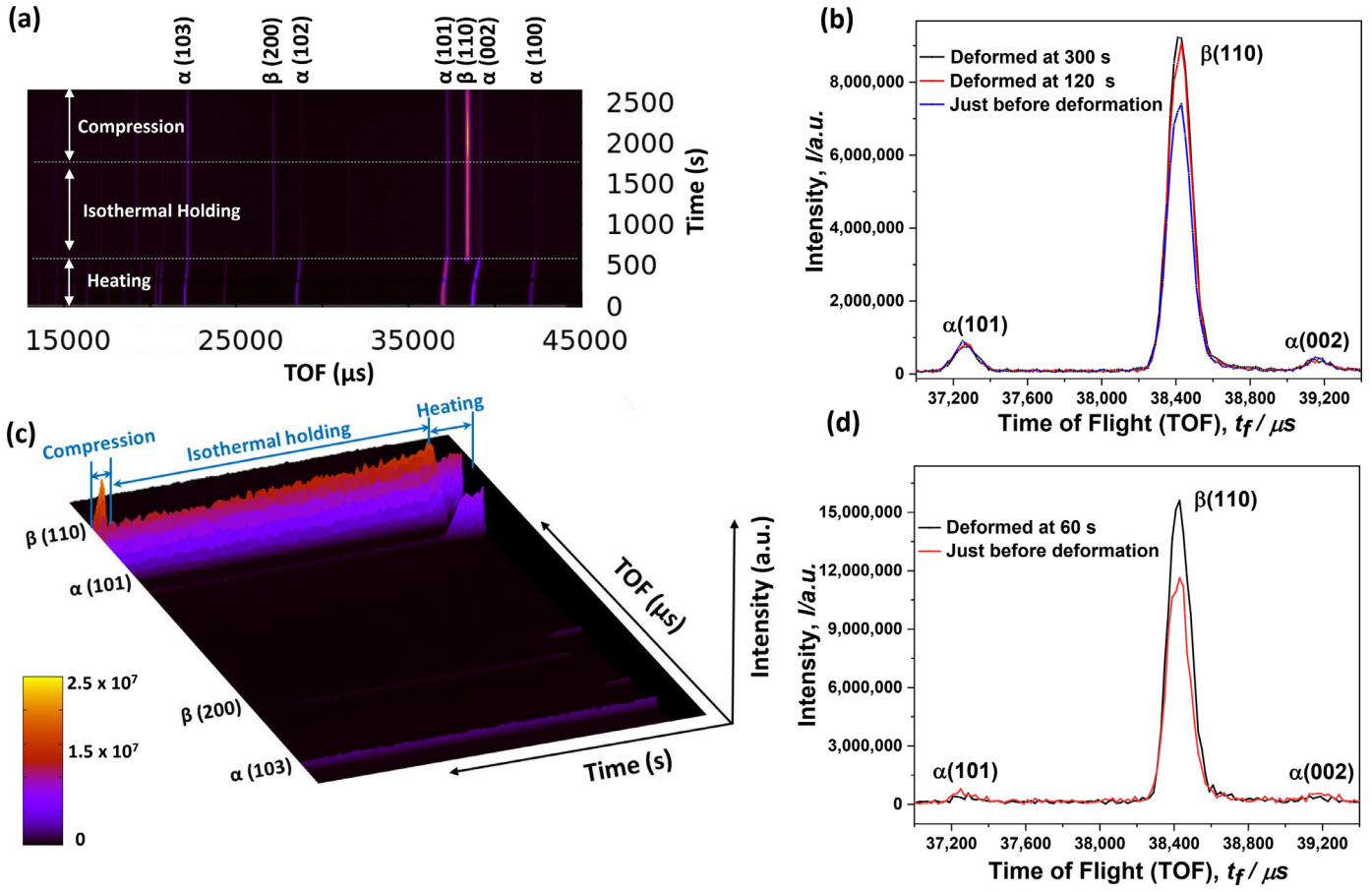

Fig. 2. (a) A two-dimensional description and (b) changes of particular peaks of the in-situ neutron diffraction result during hot-compression at 900°C and a strain rate of 0.001 s^{-1}. (c) Three-dimensional expression of the in-situ neutron diffraction profile and (d) changes of particular peaks during hot-compression at 950°C and a strain rate of 0.01 s^{-1}. In (a) and (c), the colors correspond to the intensity of peaks, according to the color bar indicated. In (b) and (d), (101) and (002) diffraction peaks of alpha phase and (110) diffraction peak of beta phase at different stages of processing are plotted for comparison. TOF indicates the time of flight of diffracted neutron, corresponding to the lattice spacing of diffracted planes [18].

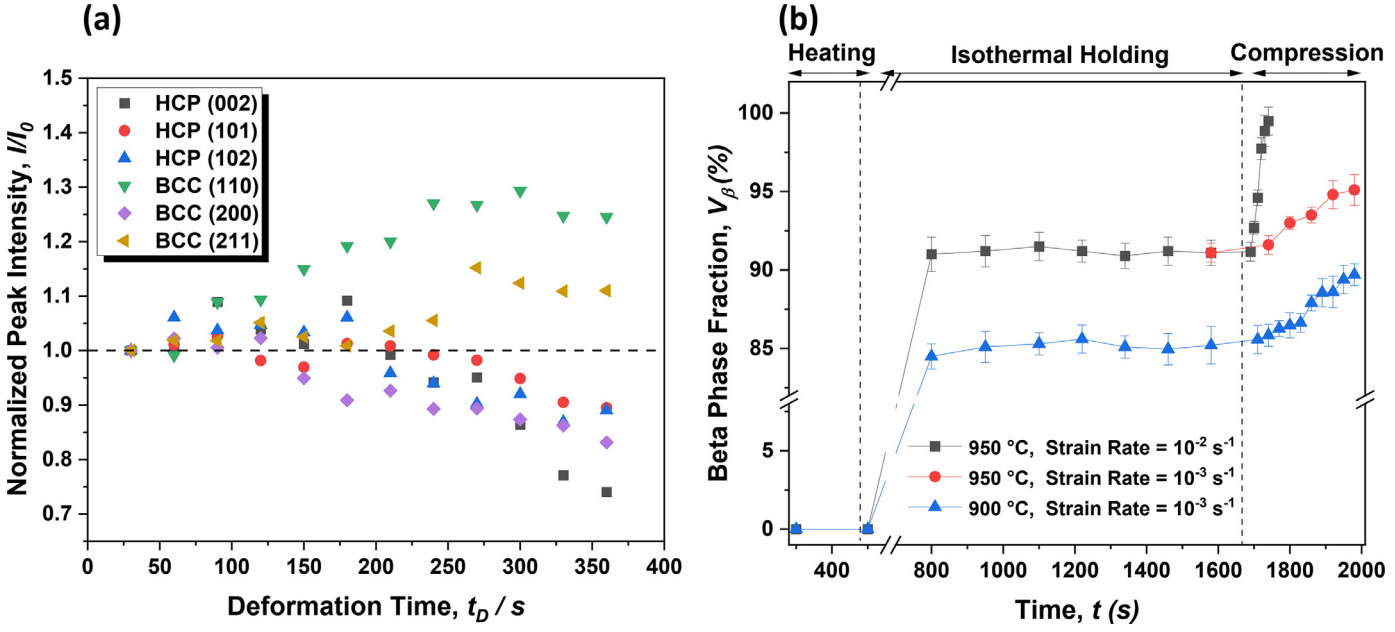

Fig. 3. (a) Normalized peak intensity of different diffraction peaks of alpha (HCP) and beta (BCC) phases as a function of the deformation time during hot-deformation at 900°C and a strain rate of 0.001 s^{-1}. (b) Changes of the volume fraction of beta phase during isothermal holding and hot-deformation at 900°C and 950°C at strain rates of 0.01 and 0.001 s^{-1}.

alpha and (200) peak of beta exhibited an initial slight increase and subsequent decrease. It should be noted that the initial slight increase in the intensity of two phases could be probably affected and caused by the increase of lattice defects and resultant local heterogeneity of lattice intervals. The decrease in the intensity of (200) peak of beta phase might be affected by crystal rotation by plastic deformation.

Changes in the volume fraction of beta phase during hot deformation at 900°C and 950°C at strain rates of 0.001 s^{-1} and 0.01 s^{-1}, respectively, are shown in Fig. 3(b). It should be noted that the phase fractions were calculated by Equation (1) using multiple peaks of two phases. For beta phase, (200) peak that showed a decreasing trend during deformation was used in addition to (110) and (211) peaks that showed increasing tends (**Fig. S1**), The volume fractions of beta phase maintained constant during isothermal holding, indicating again that the equilibrium state was achieved prior to the hot deformation. When the hot compression was carried out, the beta phase fraction increased gradually during straining. For example, 8% increase in the beta phase fraction was observed during deformation at 950°C at a strain rate of 0.01 s^{-1}, as indicated by the blue plots in Fig. 3(b). The increase of the beta volume fraction during hot-compression was also recognized under the different conditions (Fig. 3(b)), although the decreasing trend was less at the lower strain rate of 0.001 s^{-1}. As was mentioned above, the intensities of diffraction peaks could be affected by crystal rotation during hot compression more or less, although the textures of two phase were weak (**Fig. S2**). For checking the effect of this issue on the calculation of phase fractions, the MAUD software that incorporated the effects of textures on peak intensity variations was also employed to calculate the phase fractions. The result is shown in **Fig. S3** in the supplementary materials, where the beta phase fractions determined by two methods were approximately the same. It can be concluded that the effect of texture formation on the calculated phase fraction calculation is not strong and the volume fraction of beta phase certainly tends to increase during hot deformation, indicating the occurrence of dynamic transformation from alpha phase to beta phase. It should be emphasized that the dynamic transformation from alpha to beta in the present investigation was an unexpected phenomenon, since the specimens reached the equilibrium fractions of two phases and there was no driving force for the phase transformation before the hot compression. Figure 3(a) suggests that the hot deformation at higher strain rate enhances the dynamic transformation from alpha to beta, which will be discussed later.

True stress-strain curves in hot-compression at 900°C and 950°C at strain rates of 0.01 and 0.001 s^{-1} are shown in Fig. 4(a). There was an obvious flow softening (i.e., stress decrease after the peak stress) observed particularly at lower temperatures. Dynamic recovery is the predominant phenomenon in BCC beta phase associated with dislocation annihilation during hot deformation, usually giving rise to a steady state flow behavior [20]. Beta phase (BCC) is considered to be much softer than alpha phase (HCP), since the lattice strain (the phase stress) in HCP alpha was much higher than that in BCC beta, as shown in Fig. 7. The difference in strength between alpha and beta at two-phase temperatures (around 900°C – 950°C) was also investigated in the following way. The previously reported flow stresses of alpha and beta phases in single-phase temperatures of Zircalloy-4 [21] were plotted as a function of reciprocal of deformation temperature (1/T), the curves of two phases were fitted using a typical constitutive equation [21–23], and then the curves were extrapolated into alpha + beta two-phase temperature region. The result is shown as **Fig. S4** in the supplementary materials, and the figure clearly shows that the flow stress of alpha phase is much higher than that of beta phase in the alpha + beta two-phase region, which also agrees with the experimental results obtained from the in-situ neutron diffraction (Fig. 7) and our conclusion. Therefore, it can be concluded that dynamic transformation from alpha to beta can contribute to flow softening shown in Fig. 4 (a). In Fig. 4(b), changes of beta phase fraction during hot deformation are plotted against true strain in compression. It was shown that dynamic transformation was detected at an early stage of deformation, which corresponded to the initiation of flow softening. As indicated by the black curves (deformation at 950°C and 0.01 s^{-1}) in Fig. 4(a) and (b), when the flow stress reached the peak value at a strain of 0.1, approximately 2% of alpha phase had transformed to beta phase.

3.2. Diffusion associated lattice constant variation during dynamic transformation

Changes of average lattice parameters of HCP alpha and BCC beta phases during processing are shown in Fig. 5. Figure 5(a) indicates that the lattice constant of HCP alpha phase maintained approximately unchanged during holding and demonstrated an increasing trend during hot-deformation. On the other hand, the lattice constant of BCC beta phase showed an initial increase and then a decrease during hot-deformation, as indicated in Fig. 5(b). The average lattice parameters were calculated in conventional ways according to Bragg's law, using positions of diffraction peaks of each phase. Because of the diffraction geometry shown in Fig. 1, all diffraction peaks in the current experiments were obtained from crystallographic planes parallel to the compression direction. Therefore, the lattice parameters shown in Fig. 5 correspond to those in the directions perpendicular to the compression direction. In the present compression deformation, the lattice parameter naturally increased from the initial value before deformation during compression, corresponding to the elastic expansion of lattices toward the directions perpendicular to the compression direction. The change of the lattice constants in Fig. 5 corresponds to the degree of elastic deformation (expansion in the directions perpendicular to the compression direction) during compression. The decrease of the lattice constant of beta phase after the initial increase observed in Fig. 5(b) could be derived from the decrease of the flow stress (Fig. 4(a)) due to dynamic transformation.

One possible reason for the change of lattice constant by dynamic transformation is the change of chemical composition of beta phase. It has been reported in previous work [24–26] that the lattice constant of beta phase (BCC) in Ti and Zr alloys reduces with decreasing tin (Sn) content. Figure 6(a) shows a SEM micrograph of the specimen isothermally held at 950°C for 20 minutes and then quenched before the hot-deformation. As was described above, the specimen was considered to have equilibrium phase fractions before quenching. Equiaxed alpha grains that had existed in the alpha + beta state at 950°C were recognized. Beta grains transformed to alpha phase with fine plate morphologies in cooling. Figure 6(b) shows a SEM microstructure of the specimen hot-compressed to a strain of 0.7 at 950°C at a strain rate of 0.01 s^{-1} and then quenched. Equiaxed alpha grains were again observed, but the fraction of equiaxed alpha grains was obviously smaller than that in **Fig. 6** (a), which also confirmed the progress of the dynamic transformation from alpha to beta during hot deformation. It should be additionally noted that the equiaxed alpha grains only in the hot-compressed specimen (**Fig. 6** (b)) showed different appearance from those in **Fig. 6** (a). That is, the equiaxed alpha grains in **Fig. 6** (b) were outlined by layers with lighter contrast than the alpha grains, as is enlarged in **Fig. 6** (c). Sn concentrations in different local regions were measured by energy dispersive X-ray (EDX) analysis in SEM, and the results are summarized in the table inserted below Fig. 6(c). It was clearly confirmed that the Sn concentration in the light layers (1.53 wt.%) was significantly lower than that within the dark alpha grain (2.53 wt.%) but slightly higher than the (former) beta regions (1.44 wt.%) transformed to

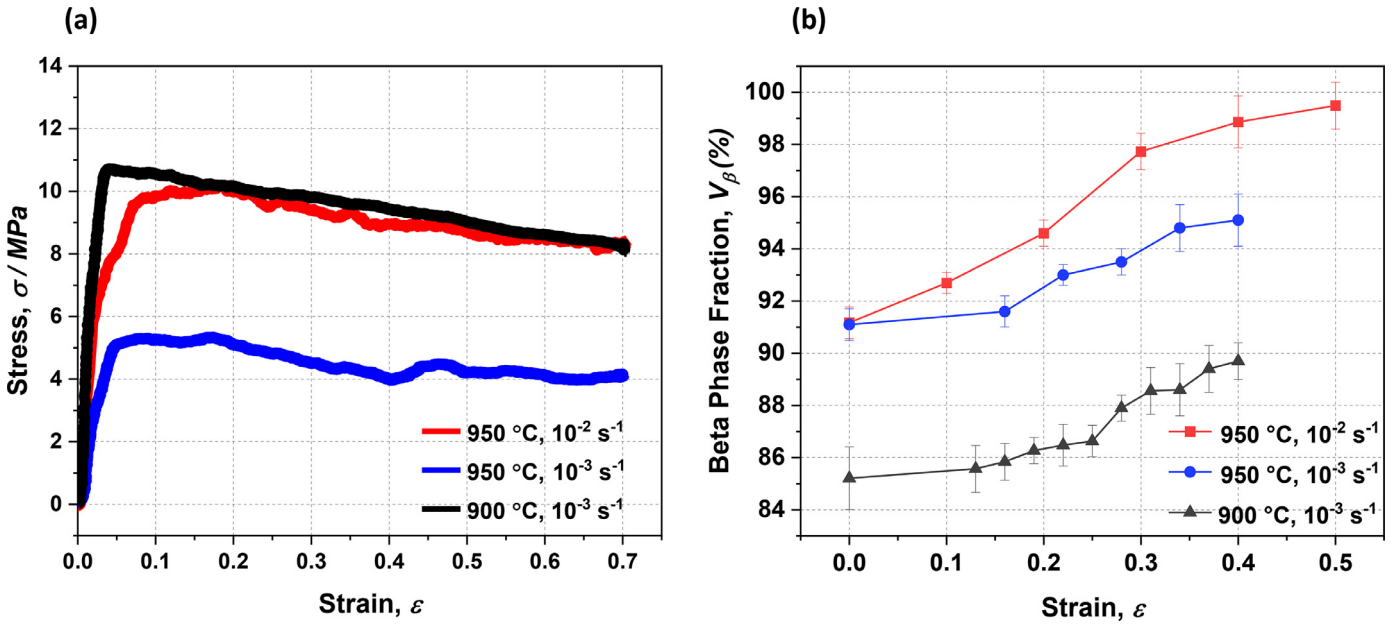

Fig. 4. (a) True stress – true strain curves in hot compression at 900°C and 950°C and strain rates of 0.01 s^{-1} and 0.001 s^{-1}. (b) Changes of beta phase fraction during hot-compression under different conditions.

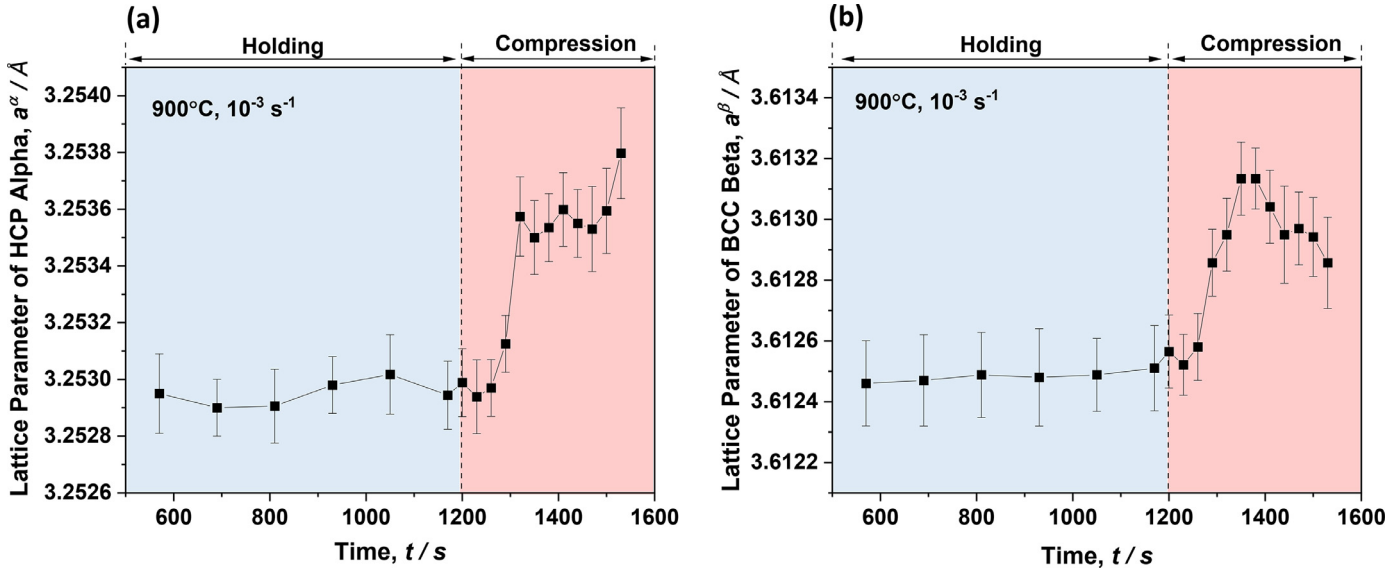

Fig. 5. Changes of the lattice constant of (a) HCP alpha phase and (b) BCC beta phase during processing. The hot-compression was carried out at 900°C and a strain rate of 0.001 s^{-1}.

fine alpha in quenching. The result indicates that dynamic transformation from alpha to beta involved Sn diffusion, and the light layers correspond to the transition regions of Sn diffusion. Note that Sn is an alpha stabilizing element in Zr alloy. Figure 6(d) represents the change of average lattice constant of BCC beta phase during processing at 950°C and 0.01 s^{-1}. Similar to Fig. 5(b), the lattice constant of beta firstly increased by hot-compression and then decreased. The first increase of the beta lattice constant corresponds to the elastic expansion of the lattice to the directions perpendicular to the compression axis, as described above. The next decrease of the lattice constant could be caused by the dynamic transformation accompanied with the gradual decrease of Sn concentration in newly formed beta phase. For confirming crystal structures in different regions, Kikuchi-line analysis was performed using electron back-scattering diffraction (EBSD) in SEM. Kikuchi diffraction patterns obtained from an equiaxed alpha grain (e), light layer (f) and transformed beta region in (c) are shown in Fig. 6(e), (f) and (g), respectively. Figure 6(e) and (f) showed nearly the same Kikuchi pattern of HCP crystal. The Kikuchi lines determined from a transformed beta region (Fig. 6(g)) showed totally different pattern from (e) and (f). The results indicate that the light layers are the HCP alpha phase having the same orientation of adjacent alpha grains, although their compositions (Sn contents) are different.

The results in the present study suggest a possible dynamic transformation process described below: During the compression deformation, Sn tends to diffuse within alpha phase along the chemical potential gradient caused by any means. When the Sn content in some area of alpha phase decreases to a certain level, dynamic transformation from alpha to beta is initiated. This might be analogous to the phase transformation from alpha to beta during heating of a titanium alloy (Ti-Mo) studied by Fu et al. using in-situ TEM observation [27]. In their work, there was an in-

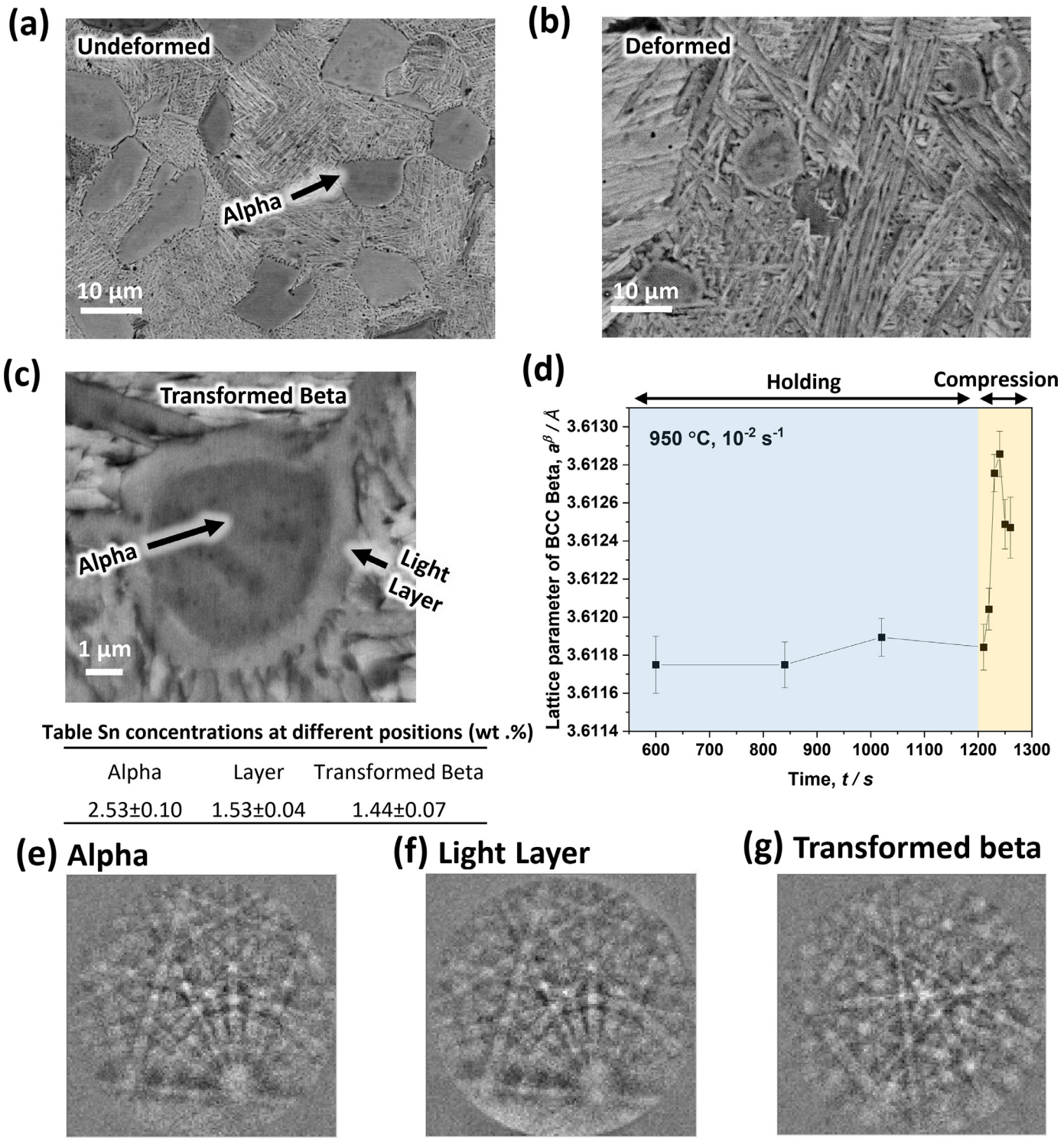

Table Sn concentrations at different positions (wt .%)

Alpha	Layer	Transformed Beta
2.53±0.10	1.53±0.04	1.44±0.07

Fig. 6. (a) SEM-BSE micrograph of the specimen held at 950°C for 20 minutes and then quenched before hot-deformation. (b) SEM-BSE image of the specimen hot-compressed to a strain of 0.7 at 950°C and 0.01 s^{-1}, and then quenched. (c) SEM-BSE micrograph of the same specimen as (b) in higher magnification. The inserted table indicates Sn concentrations at different local regions measured by EDX in SEM. (d) Change of the lattice constant of beta phase during processing at 950°C and 0.01 s^{-1}, which was derived from the in-situ neutron diffraction. (e), (f) and (g) Kikuchi patterns measured from different regions corresponding to (c), i.e., within dark equiaxed alpha grain, light layer surrounding the dark alpha grain, and transformed beta region, respectively.

termediate step during phase transformation, at which beta stabilizer (i.e., Mo in their alloy) first aggregated in a zone of alpha phase and then the alpha phase zone enriched in Mo transformed into beta phase. They claimed that such an intermediate state could lower the energy barrier of phase transformation as well. The energy barrier for phase transformation might dependent on the structure of interface between two phases. The alpha/beta interfaces in titanium and zirconium have been found to be partially coherent [28,29] and the interfacial mismatch due to the loss of coherency can be accommodated by misfit dislocations [29] or ledges [30]. These defects will increase interfacial energy and thus impede phase transformation. Recently Cui et al. [31] proposed a

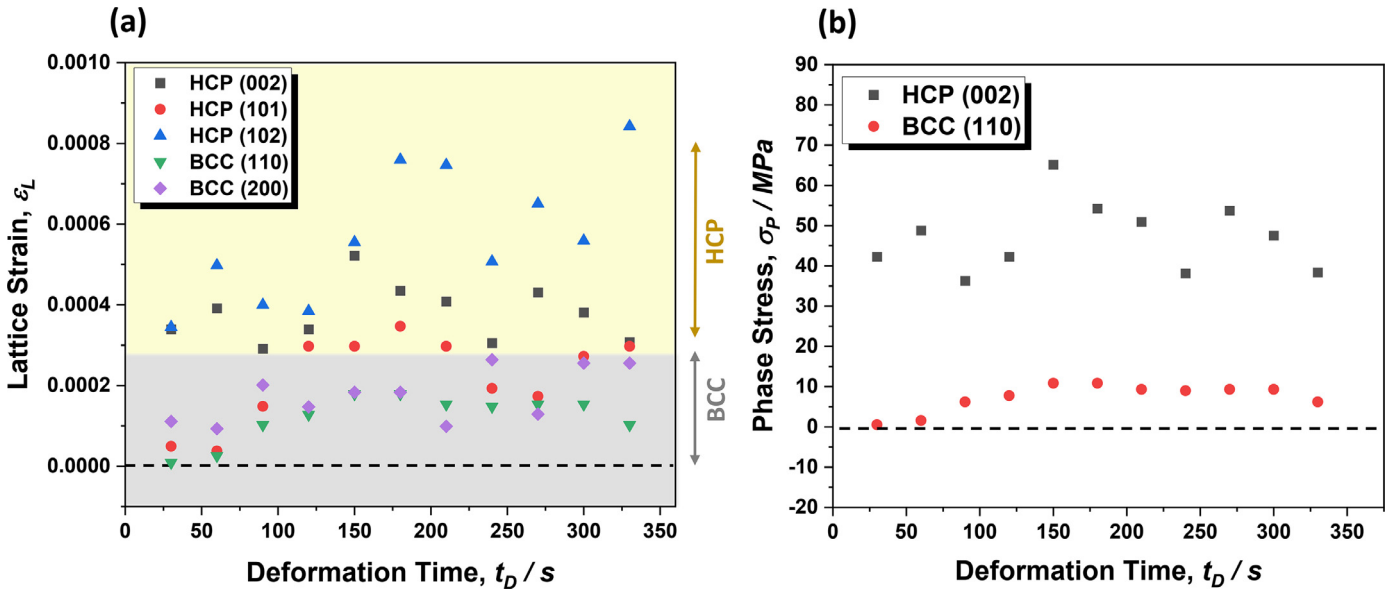

Fig. 7. Variation of (a) lattice strain and (b) phase stress of alpha and beta phases as a function of time during the hot compression at 900°C and a strain rate of 0.001 s^{-1}.

novel atomic-scale process based on the periodically differential interfacial energy and insisted that the new phase was constructed by displacive process of a group of atoms in a short range order state in Mg-Li alloy. In this process, extra driving force was required to overcome the periodic energy barriers so that a cell (a group of atoms) could transform from one metastable state to the next one via a displacive manner. Cui et al. proposed that the driving force came from thermally-activated diffusion of atoms in the transformation cell. In the current work, the authors captured a diffusion of Sn between beta and alpha phases, which seems to have a similarity to the atom-scale mechanism proposed in [31]. However, the phase transformation studied in Ref. [31] occurred without external load (i.e., static transformation), while we studied dynamic transformation in different alloy system during loading in the current study. Although we cannot assess the atom-scale mechanism proposed by Cui et al. [31] in this paper, we indicate that the driving force for the current dynamic transformation in Zr alloy is basically the elastic energy stored preferentially in alpha phase. Another possibility to explain the present results is that the light layers were formed by reverse transformation from dynamically transformed beta to alpha during cooling. The process might happen in a similar way to the epitaxial growth of alpha phase in titanium alloy [32]. Additionally, plastic accommodation of elastic stress in beta phase would also contribute to the decrease of the lattice parameter to some extent.

3.3. Mechanism of dynamic transformation

In the former sections, dynamic transformation from alpha phase to beta phase during hot-compression in alpha + beta two phase temperature was confirmed and various characteristics of the dynamic transformation were shown. In this section, mechanism of the dynamic transformation observed in the present study is discussed based on another results from the in-situ neutron diffraction and atomistic calculation. Figure 7(a) shows the variation of lattice strains (ε_{hkl}) of alpha and beta phases during hot compression at 900°C and a strain rate of 0.001 s^{-1}. The lattice strains were obtained from the peak shifts of *hkl* diffractions in the in-situ neutron investigation during hot deformation. It should be noted again here that all the diffraction peaks observed in the present in-situ neutron diffraction were obtained from the crystal planes perpendicular to the compression axis. As indicated by the yellow and grey zones, lattice strains of alpha (HCP) and beta (BCC) phases, respectively, increased gradually with the progress of hot compression. The lattice strains of alpha phase were much greater than those of beta phase, which indicates that the alpha phase plastically harder and involved higher internal (elastic) strain than beta phase. Stress partitioning between alpha and beta phases was calculated by Hooke's law using the lattice strains (ε_{hkl}) and elastic moduli along the directions perpendicular to *(hkl)* plane. Lattice stresses evaluated from (002) alpha and (110) beta (in other words, phase stresses or elastic stresses in alpha and beta phases) are plotted as a function of the deformation time in Fig. 7(b). It can be seen that the phase stresses of alpha were substantially greater than those of beta phase during the hot deformation. As elastic moduli of HCP alpha phase are generally larger than those of BCC beta phase [33,34], the elastic energy stored in alpha having higher elastic strain and larger elastic modulus must be greater than that in beta phase.

In previous works, two models have been developed to rationalize the occurrence of dynamic transformation. In the first model, stored energy in the form of lattice defects (like dislocations) is considered to give the driving force of dynamic transformation [35,36]. The second model is on the mechanical activation in which dynamic transformation is realized in a displacive manner and initiated by shear stress on habit plane [8,37]. However, both models have not yet obtained firm experimental results confirming the ideas.

In the present study, we could provide new experimental evidence in dynamic transformation, especially the stress partitioning between alpha and beta phases, from the in-situ neutron diffraction during hot deformation. Therefore, apart from two models previously proposed, we would like to start the arguments from fundamental points. The dynamic transformation should be interpreted in the context of Gibbs free energy changes from higher energy state to lower energy state, similar to conventional static transformations. The difference in dynamic transformation is the necessity to consider dynamic changes of free energy happening during deformation. Although the present results on dynamic transformation in the Zr alloy were obtained from hot deformation in alpha + beta two-phase equilibria, let us start from thermodynamics in pure metals (in pure Zr) for simplicity. Figure 8(a) schematically illustrates a temperature – Gibbs free energy (G) diagram for pure Zr. Gibbs free energies for alpha phase (G^{α}) and

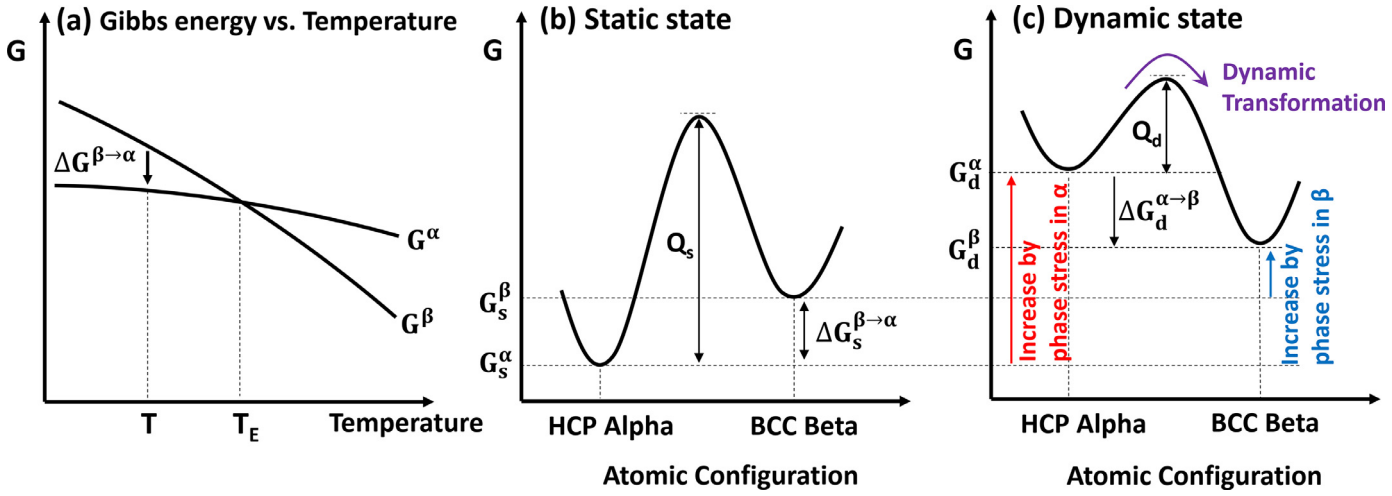

Fig. 8. Schematic illustrations showing changes of Gibbs free energy in pure Zr. (a) Gibbs free energy curves of alpha phase (G^{α}) and beta phase (G^{β}) as a function of temperature. (b) Change of Gibbs free energy of pure Zr at a temperature, T (below T_E in (a)), as a function of atomic configuration between HCP alpha and BCC beta crystals, in static state without deformation (loading). (c) Similar illustration to (b) in dynamic state under deformation (loading).

beta phase (G^{β}) both decrease with increasing temperature (T) and cross to each other at the equilibrium transformation temperature (T_E) between alpha and beta. HCP alpha phase is stable below T_E and BCC beta stable above T_E. At a temperature (T) below T_E, the driving force for the phase transformation from supercooled beta to alpha ($\Delta G^{\beta\rightarrow\alpha}$) is generated, which is the difference between free energy of alpha (G^{α}) and that of beta (G^{β}) at T. Figure 8(b) and (c) schematically demonstrate the variation of Gibbs free energy of a pure Zr system at the temperature, T, as a function of various atomic configurations between HCP alpha and BCC beta crystals. Figure 8(b) corresponds to the static state without deformation (loading). As is shown in (a), the driving force for the static transformation from beta to alpha ($\Delta G_s^{\beta\rightarrow\alpha}$) arises at this temperature (T). In the dynamic state, a load is applied to the material (system) and it changes the free energy curve (Fig. 8(c)). Loading induces elastic deformation in two phases and elastic energy is stored in each phase. The elastic deformation appears as the peak shift in diffraction peaks. The current study clearly demonstrated that alpha phase took on larger elastic deformation than beta phase, as the lattice strain (and phase stress) in HCP alpha was much higher than those in BCC beta (Fig. 7). This is because beta phase is plastically softer than alpha phase and accommodates the applied stress by plastic deformation. Consequently, hard alpha phase takes higher elastic energy than soft beta phase, which affects Gibbs free energy variation between two phases relatively. As is illustrated in Fig. 8(b) and (c), the free energy of alpha increases from G_s^{α} (static state) to G_d^{α} (dynamic state), and the free energy of beta increases from G_s^{β} to G_d^{β}, under loading. When the increase of alpha free energy (G_d^{α} - G_s^{α}) by elastic energy is sufficiently larger than that of beta free energy (G_d^{β} - G_s^{β}) (which seems to be the case in the present investigations, as was discussed in Fig. 7 based on the in-situ neutron diffraction results), the free energy of alpha (G_d^{α}) becomes higher than the free energy of beta (G_d^{β}) so that the driving force for dynamic transformation from alpha to beta ($\Delta G_d^{\alpha\rightarrow\beta}$) is generated at T, as is shown in Fig. 8(c). By the way, for inducing the dynamic transformation, the activation energy barrier (Q) must be overcome. The change of the free energy curve by loading could reduce the activation energy for the alpha to beta transformation from Q_s to Q_d, as illustrated in Fig. 8 (b) and (c), as has been shown in the explanation of *plaston* concept recently proposed for considering local nucleation of deformation carriers under loading [38–40], which would be beneficial for driving the dynamic transformation from alpha to beta. According to the work by Christian [41], the activation energy barrier for phase transformation would be lowered under deformation. In the present study, another hot-compression experiment was carried out at an alpha single-phase temperature (750°C), but no phase transformation was observed. This is probably because both $\Delta G_d^{\alpha\rightarrow\beta}$ and Q_s were naturally much larger at this temperature than those at alpha + beta two-phase temperature (900°C and 950°C), so that the increase of the free energy of alpha under loading could not generate the driving force for the phase transformation from alpha to beta or/nor overcome the activation energy barrier (Q). However, many things are still unknown about the quantitative change of the activation energy by elastic energy or stored energy in deformation. The unexpected dynamic transformation from alpha to beta during hot deformation from equilibrium state in the alpha + beta two-phase temperature in the present investigations (which corresponds to the state at T_E in **Fig. 8** for a pure metal case) could be realized in such a way.

Gibbs free energies of alpha (G_d^{α}) and beta (G_d^{β}) in the dynamic state (Fig. 8(c)) can be increased by deformation compared with those in the static state (Fig. 8(b)). As experimentally shown in Fig. 7, the elastic strain and stress in alpha phase were greater than those of beta phase in the present Zr alloy, which gave rise to higher elastic stored energy in alpha phase than that in beta phase. The increase in Gibbs free energy of (hard) alpha phase is evidently greater than that of (soft) beta phase according to the work by Jonas et al. [1,14]. Hence, it is likely that the Gibbs free energy of alpha phase (G_d^{α}) exceeds that of beta phase (G_d^{β}) during deformation, which accounts for the initiation of dynamic transformation of alpha to beta phase. This is further validated by an atomistic simulation. The calculated changes of Gibbs free energies of alpha and beta phases at 0 K are shown as a function of hydrostatic compressive pressure in Fig. 9 (a). Gibbs free energies of alpha (HCP) and beta (BCC) phases both increased with increasing the pressure, but the increasing trends are different between two phases so that two curves crosses to each other at a certain pressure. In order to demonstrate the detailed changes, the pressure range in Fig. 9 (a) was divided into three regions with different colors, and then the curves in three regions were shown in Fig. 9 (b)-(d). In the low pressure region (Fig. 9 (b)), the Gibbs free energy of alpha is always lower than that of beta phase. The medium pressure region (Fig. 9 (c)) exhibits crossing of the Gibbs free energy curves of alpha and

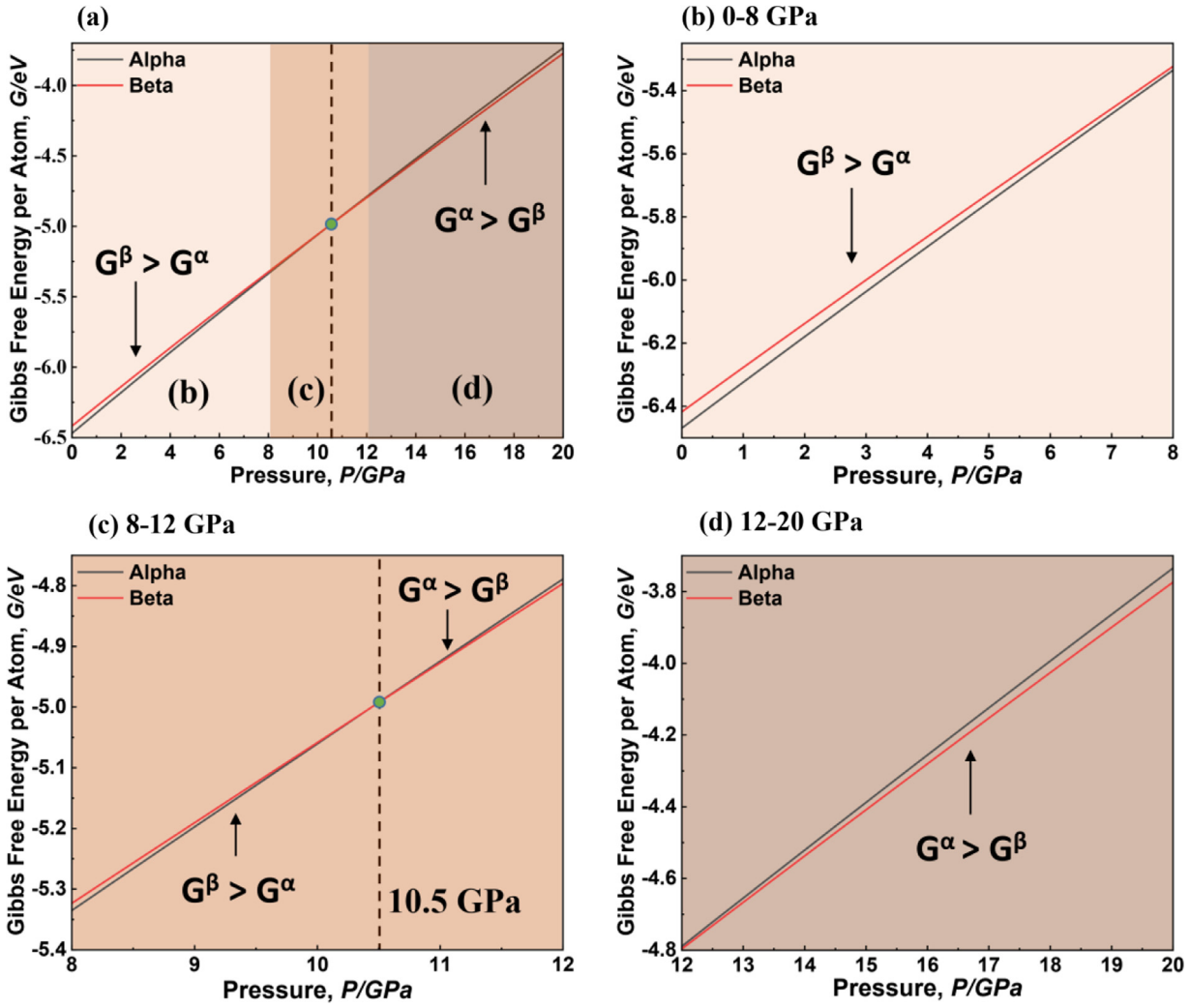

Fig. 9. (a) Changes of Gibbs free energies of alpha and beta phases are shown as a function of hydrostatic compressive pressure, calculated by the atomistic simulation. (b-d) Enlarged view of (a) in different ranges of the pressure: (b) 0 – 8 GPa, (c) 8 – 12 GPa, (d) 12 – 20 GPa.

beta at around 10.5 GPa. In the high pressure region (Fig 9 (d)), the Gibbs energy of alpha is always higher than that of beta phase. Hence, alpha phase is more stable than beta phase under lower pressure, while beta phase becomes relatively more stable than alpha phase under higher pressure. The tendency demonstrated by the calculation that the compressive pressure makes beta phase more stable than alpha phase matches well with the consideration described above for explaining the experimental result of dynamic transformation during compression in the present study

4. Conclusion

Dynamic transformation behavior in Zr alloy was thoroughly studied by the use of the in-situ neutron diffraction experiments during isothermal compression deformation at high temperatures and the atomistic simulation. The main results obtained in the current study are summarized as follows:

(1) Dynamic transformation from HCP alpha phase to BCC beta phase was directly observed and confirmed by the in-situ neutron diffraction, even though the specimen showed equilibrium phase ratios at the alpha + beta two-phase temperature before the uniaxial compression deformation. The kinetics of alpha to beta transformation and the fraction of obtained beta phase increased with increasing the deformation temperature and strain rate. Stress-strain curves in hot compression of the specimens showed gradual decreases after peak stresses at early stage of deformation, which corresponded to the increase of the beta phase produced by the dynamic transformation.

(2) The lattice parameter of alpha phase along the directions perpendicular to the compression axis showed increasing trends during the compression deformation, which indicated monotonous increase of elastic deformation in this direction. On the other hand, the lattice parameter of beta phase firstly increased and then decreased corresponding to the initiation of dynamic transformation from alpha to beta during the compression deformation. The hot compressed specimens showed a unique microstructure of alpha phase. Equiaxed alpha grains with dark contrast were surrounded by the light contrast layers. It was confirmed that the light contrast layers were alpha phase with the same crystallographic orientations of the surrounded dark alpha grains and had lower Sn concentrations than the surrounded alpha grain.

(3) Changes of the lattice strain (elastic strain) of two different phases during hot compression deformation were directly evaluated from the peak shift of diffraction peaks obtained by the in-situ neutron diffraction for the first time. HCP alpha phase always showed larger lattice strain, so that higher phase stress (elastic stress within the phase), than BCC beta phase. This indicated that the stress (load) was partitioned

into two phases and the harder alpha phase took on the higher stress than the softer beta phase. Since elastic moduli of alpha phase were larger than those of beta phase, alpha phase should include higher elastic energy than beta phase during hot deformation.

(4) It was considered that the higher elastic energy in alpha phase increased the Gibbs free energy of alpha much more than beta, and the driving force for the dynamic transformation from alpha to beta generated. The atomistic calculation showed that beta phase would have lower Gibbs free energy than alpha phase under higher hydrostatic compressive pressure, which agreed with the above mentioned consideration (Eq. 2).

Declaration of Competing Interest

The authors declare that they have no known competing financial interests or personal relationships that could have appeared to influence the work reported in this paper.

Acknowledgement

The present study was financially supported by JST CREST (JPMJCR1994), Elements Strategy Initiative for Structural Materials (ESISM, No. JPMXP0112101000), and the Grant-in-Aid for Scientific Research (No. 20H00306), all through the Ministry of Education, Culture, Sports, Science and Technology (MEXT), Japan. The neutron diffraction study was performed at the beam line 19 (TAKUMI) in J-PARC of Japan Atomic Energy Association (JAEA) under the beam time number of 2018L0401. The authors are grateful to the valuable comments from Dr. S. L. Semiatin of Air Force Research Laboratory at the Wright-Patterson Air Force Base in Dayton, Ohio, US.

Supplementary materials

Supplementary material associated with this article can be found, in the online version, at doi:10.1016/j.actamat.2022.118427.

References

[1] C. Ghosh, C. Aranas Jr, J.J. Jonas, Dynamic transformation of deformed austenite at temperatures above the Ae_3, Prog. Mater Sci. 82 (2016) 151–233.
[2] B. Guo, J.J. Jonas, Dynamic transformation during the high temperature deformation of titanium alloys, J. Alloys Compd. (2021) 161179.
[3] T. Senuma, A new thermomechanical heat treatment for grain refining in low carbon steels, in: Proc. Int. Conf. on Phys. Metallurgy of Thermomechanical Processing of Steels and Other Metals, Tokyo, 1988, pp. 200–207.
[4] L. Zhao, N. Park, Y. Tian, S. Chen, A. Shibata, N. Tsuji, Novel thermomechanical processing methods for achieving ultragrain refinement of low-carbon steel without heavy plastic deformation, Mater. Res. Lett. 5 (1) (2017) 61–68.
[5] H. Beladi, G. Kelly, P. Hodgson, Ultrafine grained structure formation in steels using dynamic strain induced transformation processing, Int. Mater. Rev. 52 (1) (2007) 14–28.
[6] H. Dong, X. Sun, Deformation induced ferrite transformation in low carbon steels, Current Opinion in Solid State and, Mater. Sci. 9 (6) (2005) 269–276.
[7] A. Shibata, Y. Takeda, N. Park, L. Zhao, S. Harjo, T. Kawasaki, W. Gong, N. Tsuji, Nature of dynamic ferrite transformation revealed by in-situ neutron diffraction analysis during thermomechanical processing, Scr. Mater. 165 (2019) 44–49.
[8] J.J. Jonas, C. Ghosh, Role of mechanical activation in the dynamic transformation of austenite, Acta Mater. 61 (16) (2013) 6125–6131.
[9] B. Guo, S. Semiatin, J.J. Jonas, Dynamic transformation during the high temperature deformation of two-phase titanium alloys, Mater. Sci. Eng. A Struct. Mater. 761 (2019) 138047.
[10] X. Ji, B. Guo, F. Jiang, H. Yu, D. Fu, J. Teng, H. Zhang, J.J. Jonas, Accelerated flow softening and dynamic transformation of Ti-6Al-4V alloy in two-phase region during hot deformation via coarsening α grain, J. Mater. Sci. Mater. Med. 36 (2020) 160–166.
[11] H. Gegel, S. Nadiv, R. Raj, Dynamic effects on flow and fracture during isothermal forging of a titanium alloy, Scr. Metall. 14 (2) (1980) 241–246.
[12] B.H. Prada, J. Mukhopadhyay, A.K. Mukherjee, Effect of strain and temperature in a superplastic Ni-modified Ti–6Al–4V Alloy, Mater. Trans. 31 (3) (1990) 200–206 JIM.
[13] J. Koike, Y. Shimoyama, I. Ohnuma, T. Okamura, R. Kainuma, K. Ishida, K. Maruyama, Stress-induced phase transformation during superplastic deformation in two-phase Ti–Al–Fe alloy, Acta Mater. 48 (9) (2000) 2059–2069.
[14] J.J. Jonas, C. Aranas Jr, A. Fall, M. Jahazi, Transformation softening in three titanium alloys, Materials & Design 113 (2017) 305–310.
[15] A.P. Thompson, H.M. Aktulga, R. Berger, D.S. Bolintineanu, W.M. Brown, P.S. Crozier, P.J. in't Veld, A. Kohlmeyer, S.G. Moore, T.D. Nguyen, LAMMPS-a flexible simulation tool for particle-based materials modeling at the atomic, meso, and continuum scales, Comput. Phys. Commun. 271 (2022) 108171.
[16] M.I. Mendelev, G.J. Ackland, Development of an interatomic potential for the simulation of phase transformations in zirconium, Philos. Mag. Lett. 87 (5) (2007) 349–359.
[17] A.V. Ivanov, V.M. Uzdin, H. Jónsson, Fast and robust algorithm for energy minimization of spin systems applied in an analysis of high temperature spin configurations in terms of skyrmion density, Comput. Phys. Commun. 260 (2021) 107749.
[18] S. MacEwen, J. Faber Jr, A. Turner, The use of time-of-flight neutron diffraction to study grain interaction stresses, Acta Metall. 31 (5) (1983) 657–676.
[19] R. Holt, The beta to alpha phase transformation in Zircaloy-4, J. Nucl. Mater. 35 (3) (1970) 322–334.
[20] S. Semiatin, V. Seetharaman, I. Weiss, Flow behavior and globularization kinetics during hot working of Ti–6Al–4V with a colony alpha microstructure, Mater Sci Eng A Struct Mater 263 (2) (1999) 257–271.
[21] Y. Cao, J. Cao, L. Wang, C. Song, F. Li, P. Zhang, High-Temperature Deformation Constitutive Model of Zircaloy-4 Based on the Support Vector Regression Algorithm during Hot Rolling, J. Mater. Eng. Perform. (2022) 1–11.
[22] F. Garofalo, An empirical relation defining the stress dependence of minimum creep rate in metals, Trans. AIME 227 (1963) 351–356.
[23] C. Aranas Jr, T. Nguyen-Minh, R. Grewal, J.J. Jonas, Flow softening-based formation of Widmanstätten ferrite in a 0.06% C steel deformed above the Ae3, ISIJ Int. 55 (1) (2015) 300–307.
[24] Y. Hao, S. Li, S. Sun, R. Yang, Effect of Zr and Sn on Young's modulus and superelasticity of Ti–Nb-based alloys, Mater. Sci. Eng. A Struct. Mater. 441 (1-2) (2006) 112–118.
[25] R.J. Pérez, C. Toffolon-Masclet, J.-M. Joubert, B. Sundman, The Zr–Sn binary system: New experimental results and thermodynamic assessment, Calphad 32 (3) (2008) 593–601.
[26] L. Wu, V.O. Kharchenko, D.O. Kharchenko, R. Pan, Energetics of binary Zr–Nb, Zr–Sn and Nb–Sn alloys and solute-vacancy binding: DFT calculations, Mater. Today Commun. 26 (2021) 101765.
[27] X. Fu, X.-D. Wang, B. Zhao, Q. Zhang, S. Sun, J.-J. Wang, W. Zhang, L. Gu, Y. Zhang, W.-Z. Zhang, Atomic-scale observation of non-classical nucleation–mediated phase transformation in a titanium alloy, Nat. Mater. (2021) 1–7.
[28] S. Banerjee, P. Mukhopadhyay, Phase transformations: examples from titanium and zirconium alloys, Elsevier, 2010.
[29] T. Furuhara, T. Ogawa, T. Maki, Atomic structure of interphase boundary of an a precipitate plate in a β Ti [sbnd] Cr alloy, Philos. Mag. Lett. 72 (3) (1995) 175–183.
[30] S. Zherebtsov, G. Salishchev, S. Lee Semiatin, Loss of coherency of the alpha/beta interface boundary in titanium alloys during deformation, Philos. Mag. Lett. 90 (12) (2010) 903–914.
[31] Y. Cui, Y. Zhang, L. Sun, M. Feygenson, M. Fan, X.-L. Wang, P.K. Liaw, I. Baker, Z. Zhang, Phase transformation via atomic-scale periodic interfacial energy, Mater. Today Phys. 24 (2022) 100668.
[32] X. Gao, W. Zeng, S. Zhang, Q. Wang, A study of epitaxial growth behaviors of equiaxed alpha phase at different cooling rates in near alpha titanium alloy, Acta Mater. 122 (2017) 298–309.
[33] D. Tromans, Elastic anisotropy of HCP metal crystals and polycrystals, Int. J. Res. Rev. Appl. Sci 6 (4) (2011) 462–483.
[34] B.-T. Wang, P. Zhang, H.-Y. Liu, W.-D. Li, P. Zhang, First-principles calculations of phase transition, elastic modulus, and superconductivity under pressure for zirconium, J. Appl. Phys. 109 (6) (2011) 063514.
[35] C. Ghosh, V.V. Basabe, J.J. Jonas, Y.-M. Kim, I.-H. Jung, S. Yue, The dynamic transformation of deformed austenite at temperatures above the Ae3, Acta Mater. 61 (7) (2013) 2348–2362.
[36] C. Zheng, N. Xiao, L. Hao, D. Li, Y. Li, Numerical simulation of dynamic strain-induced austenite–ferrite transformation in a low carbon steel, Acta Mater. 57 (10) (2009) 2956–2968.
[37] C. Aranas Jr, J.J. Jonas, Effect of Mn and Si on the dynamic transformation of austenite above the Ae3 temperature, Acta Mater. 82 (2015) 1–10.
[38] N. Tsuji, S. Ogata, H. Inui, I. Tanaka, K. Kishida, S. Gao, W. Mao, Y. Bai, R. Zheng, J.-P. Du, Strategy for managing both high strength and large ductility in structural materials–sequential nucleation of different deformation modes based on a concept of plaston, Scr. Mater. 181 (2020) 35–42.
[39] N. Tsuji, S. Ogata, H. Inui, I. Tanaka, K. Kishida, S. Gao, W. Mao, Y. Bai, R. Zheng, J.-P. Du, Corrigendum to 'Strategy for Managing Both High Strength and Large Ductility in Structural Materials-sequential nucleation of different deformation modes based on a concept of plaston'[Scripta Materialia 181 (2020) 35-42/SMM 13102], Scr. Mater. 196 (2021) 113755.
[40] I. Tanaka, N. Tsuji, H. Inui, The Plaston Concept: Plastic Deformation in Structural Materials, Springer Nature, 2022.
[41] J.W. Christian, The theory of transformations in metals and alloys, Newnes 2002.